From Point Defects in Graphene to Two-Dimensional Amorphous Carbon

J. Kotakoski[1], A. V. Krasheninnikov[1,2], U. Kaiser[3] and J. C. Meyer[3,*]
[1] *Department of Physics, University of Helsinki, P.O. Box 43, 00014 Helsinki, Finland*
[2] *Department of Applied Physics, Aalto University, P.O. Box 1100, 00076 Aalto, Finland*
[3] *Electron microscopy of materials science, University of Ulm, Germany*

While crystalline two-dimensional materials have become an experimental reality during the past few years, an amorphous 2-D material has not been reported before. Here, using electron irradiation we create an sp^2-hybridized one-atom-thick flat carbon membrane with a *random* arrangement of polygons, including four-membered carbon rings. We show how the transformation occurs step-by-step by nucleation and growth of low-energy multi-vacancy structures constructed of rotated hexagons and other polygons. Our observations, along with first-principles calculations, provide new insights to the bonding behavior of carbon and dynamics of defects in graphene. The created domains possess a band gap, which may open new possibilities for engineering graphene-based electronic devices.

PACS numbers: 68.37.Og, 81.05.ue, 64.70.Nd, 31.15.es

arXiv:1102.0174v1 [cond-mat.mtrl-sci] 1 Feb 2011

Hexagonal rings serve as the building blocks for the growing number of sp^2–bonded low-dimensional carbon structures such as graphene [1, 2] and carbon nanotubes [3]. Non-hexagonal rings usually lead to the development of non-zero curvature, *e.g.*, in fullerenes [4] and carbon nanohorns [5], where the arrangement of other polygons can be geometrically deduced via the isolated pentagon rule (IPR) [4, 6] and Euler's theorem [7]. Aberration corrected high-resolution transmission electron microscopy (AC-HRTEM) has recently allowed atomic-resolution imaging of regular carbon nanostructures and identification of defects in these materials [8–12]. Point defects, mostly vacancies, are naturally created by the energetic electrons of a TEM. However, the possibility for selectively creating topological defects representing agglomerations of non-hexagonal rings could be more desirable in the context of carbon-based electronics. [13–15]

In fact, despite the recent advances, the precise microscopic picture of the response of graphene to electron irradiation remains incomplete. Earlier experiments on curved carbon nanosystems [16, 17] have shown that they avoid under-coordinated atoms under irradiation at high temperatures via vacancy migration and coalescence. Recent experiments on graphene [12] reported only the development of holes. Theoretical studies have also predicted the appearance of small holes or formation of hæckelite-like configurations [18] or dislocations [19].

In this Letter, we report the transformation of graphene into a two-dimensional random arrangement of polygons due to continuous exposure to the electron beam with an energy just above the knock-on threshold. By carefully choosing the electron energy, we selectively enhance and suppress the underlying mechanisms of defect production. A combination of experiments and density-functional theory (DFT) calculations allows us to show that the transformation is driven by two simple mechanisms: atom ejection and bond rotation. The created defects tend to have a low formation energy and exhibit an electronic band gap. We also discover other unexpected configurations, such as stable carbon tetragons [20] which appear upon linear arrangement of di-vacancies.

Our graphene membranes were prepared by micromechanical cleavage and transfer to TEM grids [21]. Aberration-corrected HRTEM imaging was carried out in an FEI Titan 80–300, equipped with an objective-side image corrector. The microscope was operated at 80 keV and 100 keV for HRTEM imaging, and at 300 keV for irradiation. The extraction voltage of the field emission source was set to a reduced value of 2 kV in order to reduce the energy spread. For both 80 keV and 100 keV imaging, the spherical aberration was set to 20 Åμm and images were obtained at Scherzer defocus (ca. -9 nm). At these conditions, dark contrast can be directly interpreted in terms of the atomic structure.

The DFT calculations were carried out with the VASP simulation package [22, 23] using projector augmented wave potentials [24] to describe core electrons, and the generalized gradient approximation [25] for exchange and correlation. Kinetic energy cutoff for the plane waves was 500 eV, and all structures were relaxed until atomic forces were below 0.01 eV/Å. The initial structure consisted of 200 C atoms, and Brillouin zone sampling scheme of Monkhorts-Pack [26] with up to $9 \times 9 \times 1$ mesh was used to generate the k-points. Barrier calculations were carried out using the nudged elastic band method as implemented in VASP [27].

We started our experiments by monitoring *in situ* the behavior of graphene under a continuous exposure to electron irradiation using AC-HRTEM imaging with an electron energy of 100 keV, *i.e.*, just above the threshold for knock-on damage (T_d) in sp^2-bonded carbon structures [28, 29]. Fig. 1a shows a graphene structure after an electron dose of $\sim 1{\cdot}10^{10}$ e^-/nm^2. Contrary to the expectations, the structure does not predominantly consist

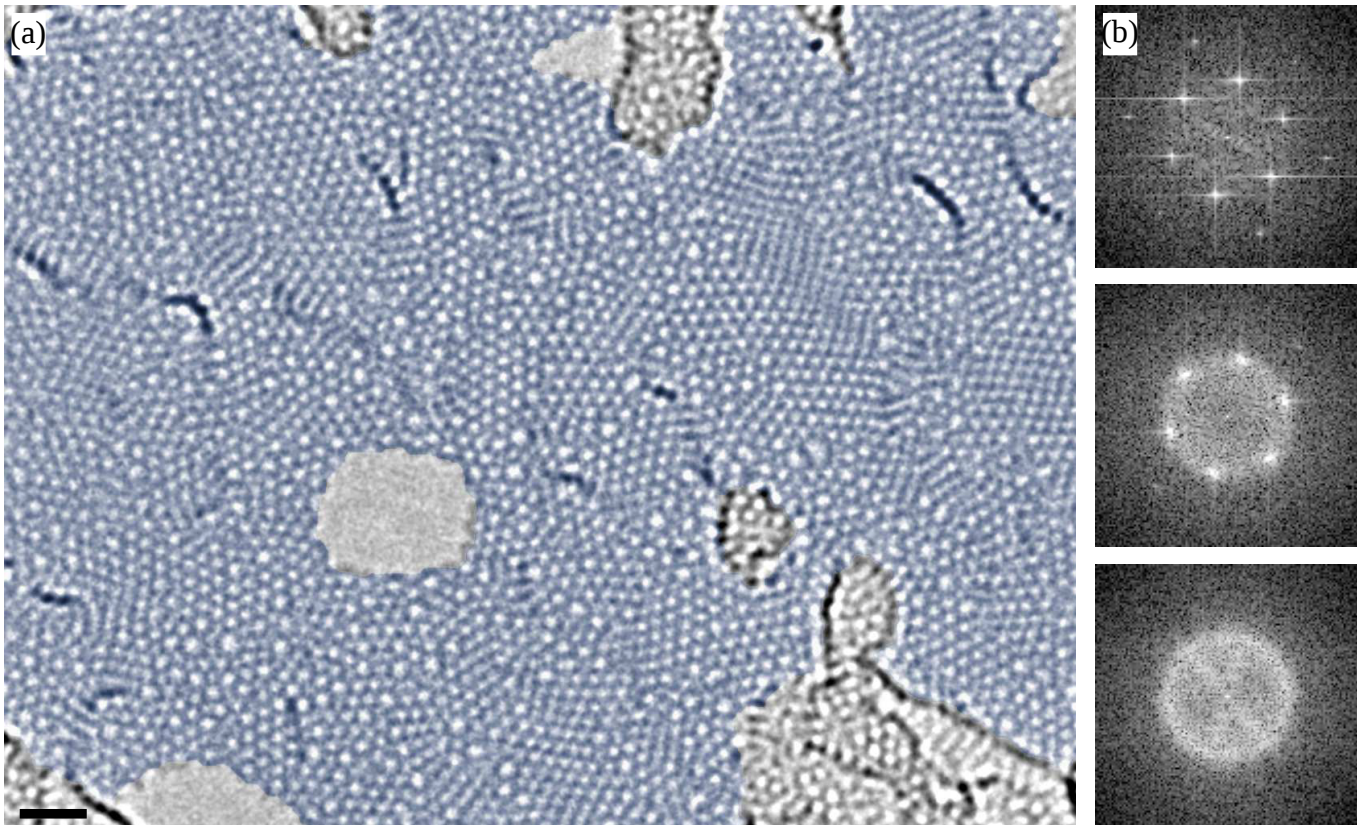

Figure 1. (a) (Color online) Amorphous two-dimensional sp^2-bonded carbon membrane created by a high-dose exposure of graphene to 100 keV electron irradiation in an HRTEM. The blue colored area is a single-layer carbon structure. Scale bar is 1 nm. (b) Fourier transforms (power spectra) from HRTEM images of the initial graphene configuration (top), an intermediate configuration (center), and of the amorphous 2D carbon (bottom).

of holes or collapse into a 3D object. Instead, it has remained as a coherent single-layer membrane composed of a random patch of polygons. Holes have also formed, but only on a small fraction of the area. The Fourier transform of the image shows that the resulting structure is completely amorphous (Fig 1b).

In order to understand the mechanisms behind the transformation, we separated them by varying the electron beam energy. To observe how a defected graphene sheet reacts to an electron beam when atomic ejections are prohibited by a low enough electron energy, we created initial damage in a graphene sheet by brief 300 keV irradiation, and then studied the generated structures at 80 keV. Now only under-coordinated atoms can be ejected (T_d for a sp^2–bonded C is about 18–20 eV [28, 29], whereas DFT calculations predict a T_d of $\sim$14 eV for a two-coordinated C). However, bond re-organization is possible, as activation energies for bond rotations in sp^2-bonded carbon structures are in the range of 4–10 eV [30, 31], depending on the local atomic configuration. Correspondingly, in pristine graphene, bond rotations are occasionally observed under 80 keV irradiation [9] (Fig. 2a,b), resulting in the formation of the Stone-Wales defect [32]. In all observed cases continued exposure reversed this transition in pristine graphene. However, defect structures, *e.g.*, di-vacancies, can convert between different configurations (Fig. 2d-f) via bond rotations. According to our DFT simulations, the barriers for bond rotations in these structures are 5–6 eV, which excludes thermally activated migration.

In Fig. 3a–d we present evolution of a more complex defect structure. The defects created by an electron beam are predominantly mono-vacancies, which quickly convert to di-vacancies due to a higher probability for under-coordinated atoms to be ejected, as noted above. Here (Fig. 3a), a brief exposure to a 300 keV beam (dose $\sim 10^7$ e^-/nm^2) has created an isolated V_2(555-777) and a defect with 4 missing carbon atoms (two connected di-vacancies). During the image sequence, the 80 keV electron beam causes the structure to re-organize via bond rotations. The V_2(555-777) turns first into a V_2(5-8-5) (Fig. 3b and then a dislocation dipole (Fig. 3c), before forming a defect composed of clustered di-vacancies (Fig. 3d). Fig. 3a–d also present two frequently observed linear arrangements of di-vacancies.

Because atom ejection occurs at random positions, va-

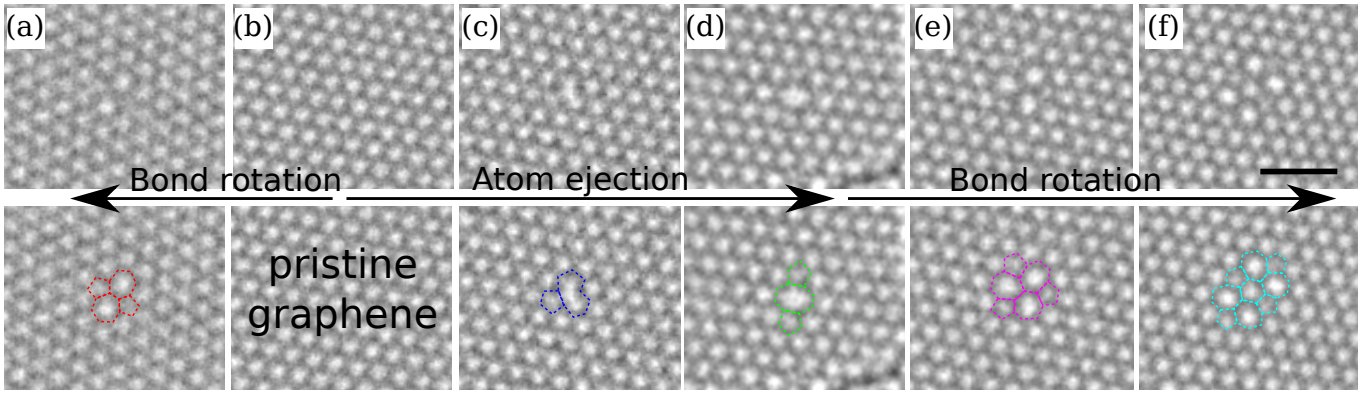

Figure 2. (Color online) Elementary defects and frequently observed defect transformations under irradiation. Atomic bonds are superimposed on the defected areas in the bottom row. Creation of the defects can be explained by atom ejection and re-organization of bonds via bond rotation. (a) Stone-Wales defect, (b) defect-free graphene, (c) V_1(5-9) single vacancy, (d) V_2(5-8-5) di-vacancy, (e) V_2(555-777) di-vacancy, (f) V_2(5555-6-7777) di-vacancy. Scale bar is 1nm.

cancies initially appear randomly in the area exposed to the electron beam. However, during lower-energy exposure (*e.g.*, 80 keV), these defects travel via a re-bonding mechanism, which is illustrated in Fig. 3e. Each migration step is initiated by a single electron impact from which the atom obtains energy slightly below T_d. In other words, electron irradiation provides the activation energy to drive the system from a local energy minimum into another one, in our case predominantly via (reversible) bond rotations (Fig. 2d-f, Fig. 3a-d). This can be clearly seen in video S4 in Ref. 33 (partially shown in Fig. 3a–d), where the configuration changes frequently until it arrives in the more stable configuration composed of three aligned double-vacancies.

Individual transitions can also lead to higher energy structures. For example, the intermediate states for the di-vacancy migration [dislocation dipole (Fig. 3c) and V_2(555-777) (Fig. 3a)] have formation energies E_f which differ from that of the V_2(5-8-5) by $\sim +3.72$ eV and ~ -0.66 eV, respectively. Aligning di-vacancies along the zigzag direction of the lattice (Fig. 3d), ~ 1.32 eV of energy is gained per a di-vacancy pair, as compared to isolated di-vacancies. When the alignment appears along the armchair direction (Fig. 3a–c), the energy gain is 2.01 eV. In this case, a tetragon is formed where the two pentagons of the adjacent di-vacancies would overlap. HRTEM simulation of the DFT-optimized structure of the defect is in excellent agreement with the experimental image [33]. Note that sp^2-bonded carbon tetragons in molecules, as in cyclobutadiene, can be stabilized only at low temperatures and when the molecules are embedded into a matrix [20]. In our case they are stabilized by the surrounding graphene lattice, as theoretically predicted for nanotubes [34].

Under 100 keV irradiation, atom ejection occurs at a very slow rate, so that changes in the atomic network are sufficiently slow to be precisely resolved. Therefore, the reconstruction of vacancy defects via bond rotations can be monitored immediately after a vacancy is generated. An example is presented in Fig. 4. The initial configuration (Fig. 4a) consists of three di-vacancies in the armchair orientation (formed prior to recording the first image). In the recorded images, the structure loses atoms until 24 atoms are missing. Several remarkable configurational changes are found in this image sequence. Fig. 4a–c shows a collapse of linearly clustered defects into an apparently less defective structure with a dislocation dipole. This corresponds to the prediction of Jeong *et al.* [19] that the dislocation dipole is favored over a large multi-vacancy. However, this requires a linear arrangement of vacancies. Fig. 4c–d shows the loss of four additional atoms. Two of them gave rise to an additional di-vacancy; the other two contributed to the separation of the dislocation cores (the rotated hexagon, clustered with a Stone-Wales defect, constitutes a dislocation core). During continued irradiation, we see the formation of a cluster of rotated hexagons surrounded by a chain of alternating pentagons and heptagons (Fig. 4e–h). Such configurations, rotated by 30° with respect to the original lattice and matched by pentagons and heptagons to the zigzag lattice direction, appear to be the preferred way to incorporate missing atoms in the graphene structure. Due to the matching numbers of pentagons and heptagons – and hence cancellation of negative and positive curvature – these structures remain flat.

To understand the driving force for the transformations, we calculated E_f for the simplest defect structures matching the obverved trend of forming a rotated hexagon kernel. The lowest-energy tetra-vacancy (four missing atoms) can be created by combining two V_2(5555-6-7777) di-vacancies, whereas the hexa-vacancy (six missing atom) requires three of these defects (Fig. 5a). Remarkably, these configurations have the lowest E_f of any reported vacancy structures with equal number of miss-

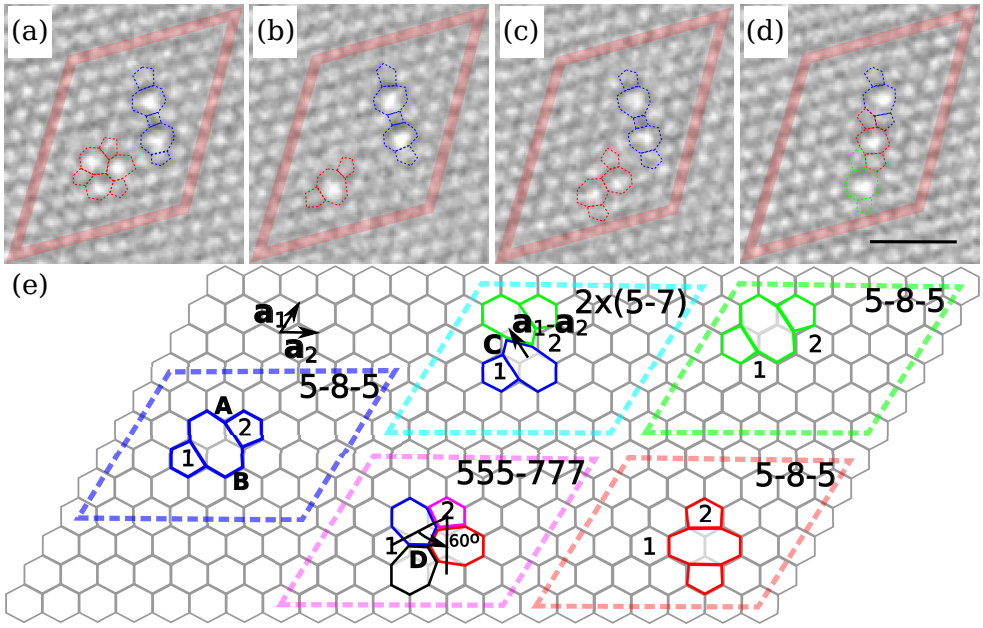

Figure 3. (Color online) (a–d) Electron beam driven di-vacancy migration observed at 80 keV. In (e), the changes in the bond configuration required for allowing the migration of a di-vacancy are shown. Transformation V_2(5-8-5)→2×(5-7) is initiated by rotating bond A, and V_2(5-8-5)→V_2(555-777) by rotating bond B. Rotating bonds C and D will lead to the final V_2(5-8-5) structures. In the first case the defect has moved by $\mathbf{a}_1 - \mathbf{a}_2$, and in the second case it has rotated by 60° around pentagon 2. The original TEM images without overlays for panels (a-d) are presented in Ref. [33].

ing atoms in graphene (E_f per missing atom multiplied by the number of missing atoms are $\sim$ 4×3.14 eV and $\sim$ 6×2.50 eV). A hole with six missing atoms has a formation energy of $\sim$ 6×3.15 eV, while for a dislocation and a hæckelite-like structure values of $\sim$ 6×3.72 eV and $\sim$ 6×2.64 eV have been reported [19], respectively. Evidently, the rotated hexagon defects spawn the family of lowest energy multi-vacancies in graphene. In contrast to what was recently shown for the zigzag-oriented di-vacancies [14], these structures open a band gap in graphene, as can be seen from the density of states (Fig. 5b). The calculated band gap is in the order of 200 meV. This value is possibly underestimated within the used GGA approximation, and advanced DFT methods are likely to give a higher value [35].

To conclude, we have shown how an electron beam can be used to selectively suppress and enhance bond rotations and atom removal in graphene. We demonstrated that irradiation at electron energies just above the threshold for atom displacement turns graphene not into a "perforated graphene" but a two-dimensional coherent amorphous membrane composed of sp^2–hybridized carbon atoms. This membrane grows through nucleation and expansion of defects which result from electron beam–driven di-vacancy migration and agglomeration. These defect configurations predominantly consist of a 30° rotated kernel of hexagons surrounded by a chain of alternating pentagons and heptagons. These defects are the energetically favored way for the graphene lattice to accommodate missing atoms, and have a semiconducting nature. Since several of the presented examples of the two-dimensional sp^2–hybridized defect configurations violate the IPR, due to increased reactivity [6, 36], they may be exploited for functionalization of graphene. We also showed unambiguous evidence for four-membered carbon rings in graphitic structures. Clearly, despite of the large amount of research, the richness of carbon chemistry continues to provide surprises. More examples of the observed structures and videos of the complete TEM image series are presented in Ref. [33].

We acknowledge support by the German Research Foundation (DFG) and the German Ministry of Science, Research and the Arts (MWK) of the state Baden-Wuerttemberg within the SALVE (sub angstrom low voltage electron microscopy) project and by the Academy of Finland through several projects. We are grateful for the generous grants of computer time provided by CSC Finland.

* Current address: University of Vienna, Department of Physics, Strudlhofgasse 4, 1090 Vienna, Austria

[1] K. S. Novoselov, A. K. Geim, S. V. Morozov, D. Jiang, Y. Zhang, S. V. Dubonos, I. V. Grigorieva, and A. A. Firsov, Science **306**, 666 (2004).

[2] K. S. Novoselov, D. Jiang, F. Shedin, T. J. Booth, V. V. Khotkevich, S. V. Morozov, and A. K. Geim, PNAS **102**,

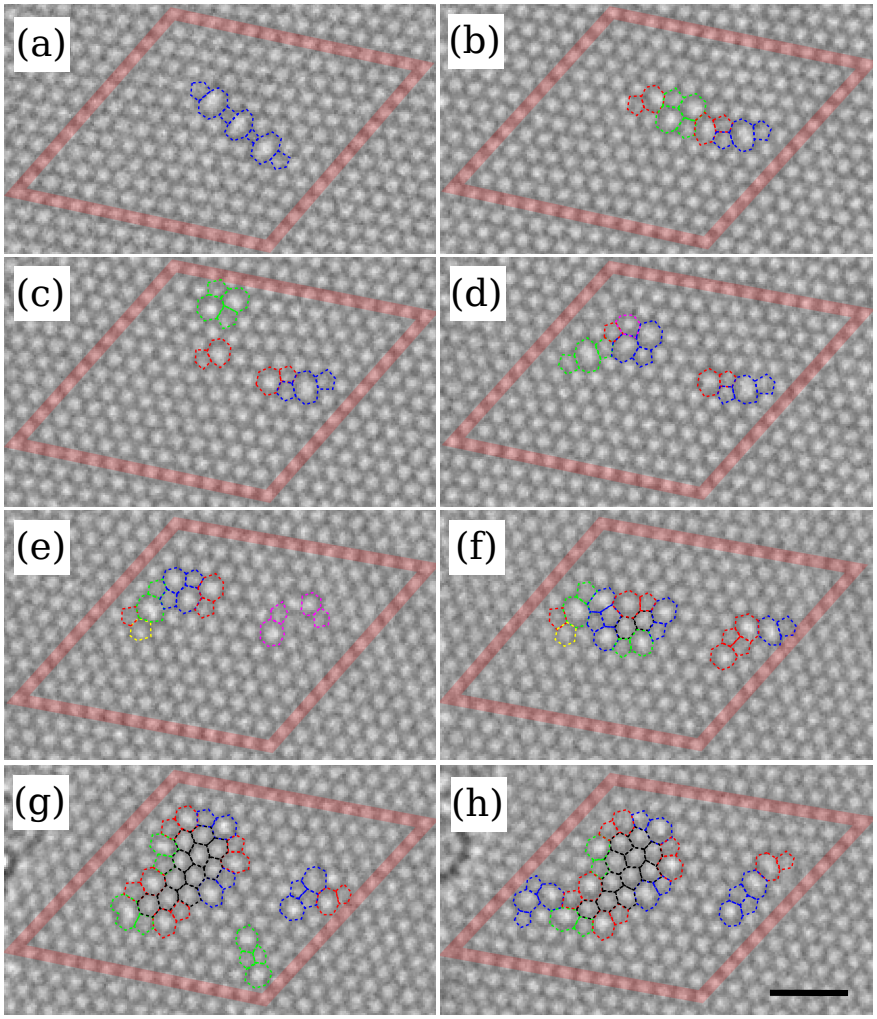

Figure 4. (Color online) Formation of rotated hexagon-kernels in multi-vacancy structures under a 100 keV electron beam. Scale bar is 1nm. The original TEM images without overlays are presented in Ref. [33].

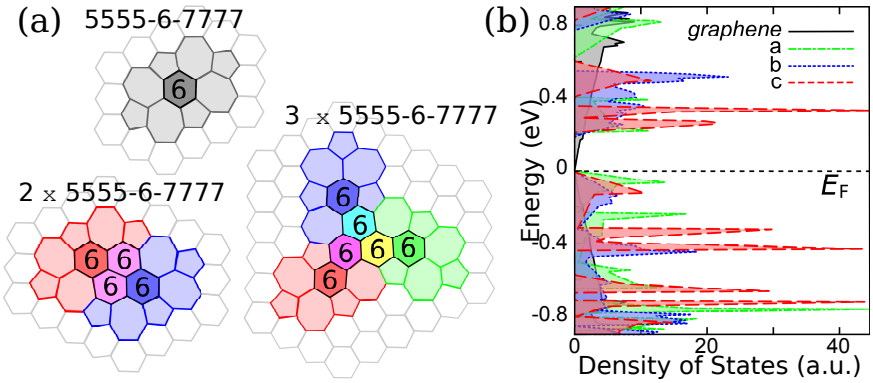

Figure 5. (Color online) Idealized rotated-hexagon defects (a) formed from one, two and three V_2(5555-6-7777) di-vacancy defects, as optimized with DFT calculations. Electronic density of states (b) for pristine graphene and the structures presented in panel (a).

10451 (2005).
[3] S. Iijima, Nature **354**, 56 (1991).
[4] H. W. Kroto, Nature **329**, 529 (1987).
[5] S. Iijima, M. Yudasaka, R. Yamada, S. Bandow, K. Suenaga, F. Kokai, and K. Takahashi, Chemical Physics Letters **309**, 165 (1999).

[6] T. G. Schmalz, W. A. Seitz, D. J. Klein, and G. E. Hite, J. Am. Chem. Soc. **110**, 1113 (1988).
[7] H. Terrones and A. L. Mackay, Carbon **30**, 1251 (1992).
[8] A. Hashimoto, K. Suenaga, A. Gloter, K. Urita, and S. Iijima, Nature (London) **430**, 870 (2004).
[9] J. C. Meyer, C. Kisielowski, R. Erni, M. D. Rossell, M. F. Crommie, and A. Zettl, Nano Letters **8**, 3582 (2008).
[10] M. H. Gass, U. Bangert, A. L. Bleloch, P. Wang, R. R. Nair, and G. K., Nat Nano **3**, 676 (2008).
[11] C. O. Girit *et al.*, Science **323**, 1705 (2009).
[12] J. H. Warner, M. H. Rummeli, L. Ge, T. Gemming, B. Montanari, N. M. Harrison, B. Buchner, and G. A. D. Briggs, Nat Nano **4**, 500 (2009).
[13] A. H. Castro Neto, F. Guinea, N. M. R. Peres, K. S. Novoselov, and A. K. Geim, Rev. Mod. Phys. **81**, 109 (2009).
[14] J. Lahiri, Y. Lin, P. Bozkurt, I. I. Oleynik, and M. Batzill, Nat Nano **5**, 326 (2010).
[15] O. V. Yazyev and S. G. Louie, Nat Mater **9**, 806 (2010).
[16] L. Sun, F. Banhart, A. V. Krasheninnikov, J. A. Rodríguez-Manzo, M. Terrones, and P. M. Ajayan, Science **312**, 1199 (2006).
[17] L. Sun, A. V. Krasheninnikov, T. Ahlgren, K. Nordlund, and F. Banhart, Phys. Rev. Lett. **101**, 156101 (2008).
[18] H. Terrones, M. Terrones, E. Hernández, N. Grobert, J.-C. Charlier, and P. M. Ajayan, Phys. Rev. Lett. **84**, 1716 (2000).
[19] B. W. Jeong, J. Ihm, and G.-D. Lee, Phys. Rev. B **78**, 165403 (2008).
[20] Y.-M. Legrand, A. v. d. Lee, and M. Barboiu, Science **329**, 299 (2010).
[21] J. C. Meyer, C. O. Girit, M. F. Crommie, and A. Zettl, Appl. Phys. Lett. **92**, 123110 (2008).
[22] G. Kresse and J. Furthmüller, Comput. Mat. Sci. **6**, 15 (1996).
[23] G. Kresse and J. Furthmüller, Phys. Rev. B **54**, 11169 (1996).
[24] P. E. Blöchl, Phys. Rev. B **50**, 17953 (1994).
[25] J. P. Perdew, K. Burke, and M. Ernzerhof, Phys. Rev. Lett. **77**, 3865 (1996).
[26] H. J. Monkhorst and J. D. Pack, Phys. Rev. B **13**, 5188 (1976).
[27] G. Henkelman, B. P. Uberuaga, and H. Jónsson, J. Chem. Phys. **113**, 9901 (2000).
[28] F. Banhart, Rep. Prog. Phys. **62**, 1181 (1999).
[29] B. W. Smith and D. E. Luzzi, J. Appl. Phys. **90**, 3509 (2001).
[30] C. P. Ewels, M. I. Heggie, and P. R. Briddon, Chem. Phys. Lett. **351**, 178 (2002).
[31] L. Li, S. Reich, and J. Robertson, Phys. Rev. B **72**, 184109 (2005).
[32] A. J. Stone and D. J. Wales, Chem. Phys. Lett. **128**, 501 (1986).
[33] See EPAPS Document No. to-be-inserted for experimental videos and additional images. For more information on EPAPS, see http://www.aip.org/pubservs/epaps.html.
[34] W. Orellana, Phys. Rev. B **80**, 075421 (2009).
[35] D. J. Appelhans, Z. Lin, and M. T. Lusk, Phys. Rev. B **82**, 073410 (2010).
[36] Y.-Z. Tan, S.-Y. Xie, R.-B. Huang, and L.-S. Zheng, Nat Chem **1**, 450 (2009).
[37] P. Thévenaz, U. Ruttimann, and M. Unser, IEEE Transactions on Image Processing **7**, 27 (1998).

METHODS

As described in the main article, graphene membranes were prepared by micro-mechanical cleavage and transfer to TEM grids [21]. Aberration-corrected HRTEM imaging was carried out in an FEI Titan 80–300, equipped with an objective-side image corrector. The microscope was operated at 80 keV and 100 keV for HRTEM imaging, and at 300 keV for irradiation. The extraction voltage of the field emission source was set to a reduced value of 2 kV in order to reduce the energy spread. For both 80 keV and 100 keV imaging, the spherical aberration was set to 20 μm and images were obtained at Scherzer defocus (ca. -9 nm). At these conditions, dark contrast can be directly interpreted in terms of the atomic structure. Image sequences were recorded on the CCD camera with exposure times ranging from 1 s to 3 s and intervals between 4 s and 8 s, and a pixel size of 0.2 Å. The effect of slightly uneven illumination is removed by normalization (division) of the image to a strongly blurred copy of the same image, effectively removing long-range variations. Drift-compensation is done using the Stackreg plugin for the ImageJ software [37]. We show individual exposures as well as averages of a few frames (up to 10). This is because we have used different beam current densities, in order to test for possible dose rate effects (within the 100 keV, simultaneous imaging and defect generation experiment). The configurations described here can be discerned in individual exposures if ca. 10^4 counts per pixel at 0.2 Å pixel size are used. With a high beam current density, this is possible in 1 s exposures (corresponding to a total dose of ca. $10^5 \frac{e^-}{\text{Å}^2}$ per image, and a dose rate of $10^5 \frac{e^-}{\text{Å}^2 \cdot s}$). At lower current densities, the same dose was spread over several exposures, so that sample drift could be compensated (individual exposures could not be longer than 3 s due to sample drift). The lowest dose rate was ca. $3 \cdot 10^3 \frac{e^-}{\text{Å}^2 \cdot s}$. Within our dose rate range, density and shape of defects appears to depend only on the total dose.

Formation energy of a structure in our DFT calculations was defined in the usual way as

$$E_f(V_n) = E_{\text{tot}}(V_n) - E_{\text{tot}}^{\text{gr}} + n\mu_{\text{gr}}, \qquad (1)$$

where $E_{\text{tot}}(V_n)$ and $E_{\text{tot}}^{\text{gr}}$ are the total energies of the structure with the defect (n missing atoms) and the same supercell without the defect, respectively, and μ_{gr} is the chemical potential of a carbon atom in pristine graphene. The semi-conducting features of the defects were consistently observed with varying number of k-kpoints used in calculating the electronic density of states.

FURTHER IMAGES

For clarity we show here the TEM images of the main article without stucture overlay, and also a few addi-

tional TEM images. Fig. 6 shows several di-vacancy (DV) defects in linear alignment. In particular, the carbon tetragon is always reproduced when the DVs are aligned along the armchair direction of the graphene lattice. Fig. 7 shows a comparison between a HRTEM image simulation based on a DFT-optimized structure and an actual HRTEM image for the armchair alignment of di-vacancies, which contains the carbon tetragons.

In Fig. 8, we show the panels a–d from the Figure 3 of the main article with and without overlays. These images are also contained in Supplementary video S2. In Fig. 9 we show panels a–h from the Figure 4 of the main article with and without overlay (the corresponding time series is shown in Supplementary video S3).

In Fig. 10, we show two additional images where a defect with a rotated hexagon kernel was generated from clusters of multiple vacancies. These configurations were created by a short 300 keV exposure and subsequent imaging at 80 keV. It should be noted that the rotated hexagon kernels appear in the larger vacancy clusters in both of our experiments (100 keV irradiation with simultaneous imaging as in Figure 4 of the main article, and the 300 keV/80 keV combination as shown in Fig. 10).

DESCRIPTION OF THE SUPPLEMENTARY VIDEOS

Supplementary video S1: Generation and transformation of defects under 100 keV irradiation. Each frame is an average of 2 CCD exposures. Note the continuous increase in defect density and partial amorphization of the membrane.

Supplementary video S2: Further transformation of graphene to a 2D amorphous membrane under 100 keV irradiation. In terms of total dose, it can be considered as a continuation of video S4 (although sample region is different). Each frame shows an individual CCD exposure. Note that the entire clean graphene area becomes amorphous while remaining one-atom thick, and beam-generated holes make up only a small fraction of the area.

Supplementary video S3: Two isolated di-vacancies, generated by brief 300 keV irradiation and observed at 80 keV. The di-vacancies migrate under the beam and transform between the V_2(5-8-5), V_2(555-777) and V_2(5555-6-7777) configurations multiple times. The video shows individual exposures in each frame.

Supplementary video S4: A cluster of several vacancy defects, generated by brief 300 keV irradiation and observed at 80 keV. The video shows individual exposures in each frame. The configuration changes continuously until the final, linear aligned di-vancy configuration is observed and stable throughout several exposures (frames 22–29). Frames 30–36 are duplicates of frame 29 in order to show the final configuration as a still image at the end.

Supplementary video S5: Generation and transformation of defects under 100 keV irradiation. Each frame is an average of 10 CCD exposures (recorded at a lower current density). This video shows the generation of the rotated hexagon kernel as in Figure 4 of the main article. The rotated hexagon kernel is highlighted as overlay in frames 28–31.

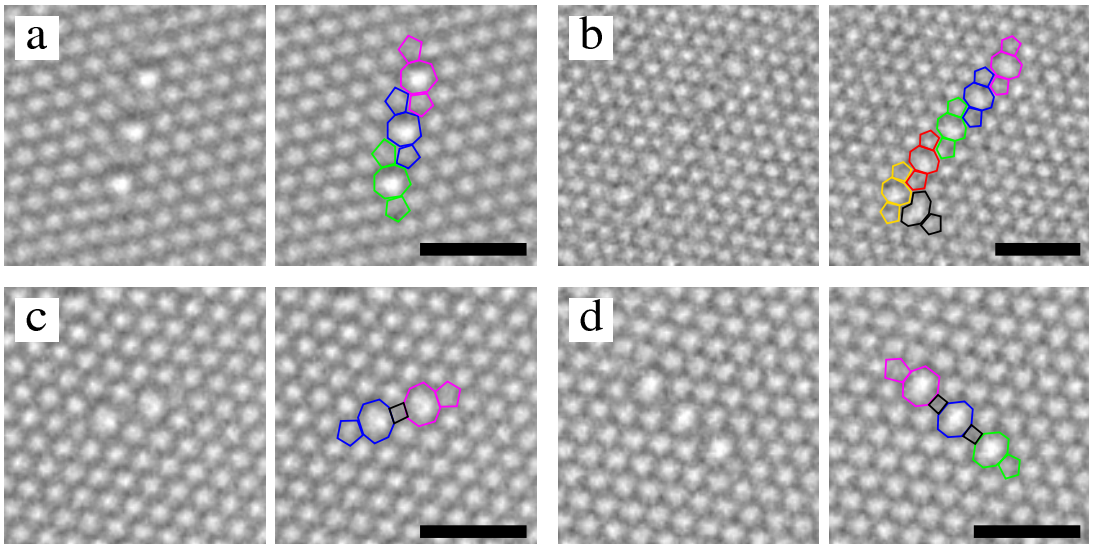

Figure 6. Images of di-vacancy (DV) defects in linear alignment, shown with and without structure overlay in each case. (a) Three DVs aligned along the zigzag direction of the graphene lattice. (b) Five DVs aligned in zigzag direction, clustered with a single vacancy (black). (c) Two DVs aligned along the armchair direction, forming a carbon tetragon at their intersection. (d) Three DVs aligned along the armchair direction, forming two carbon tetragons. All scale bars are 1 nm.

Figure 7. DFT-optimized structure of the defect with two tetragons (a), HRTEM simulation based on the DFT-structure (b) and the HRTEM image of the same structure for comparison (c). Scale bar is 1 nm.

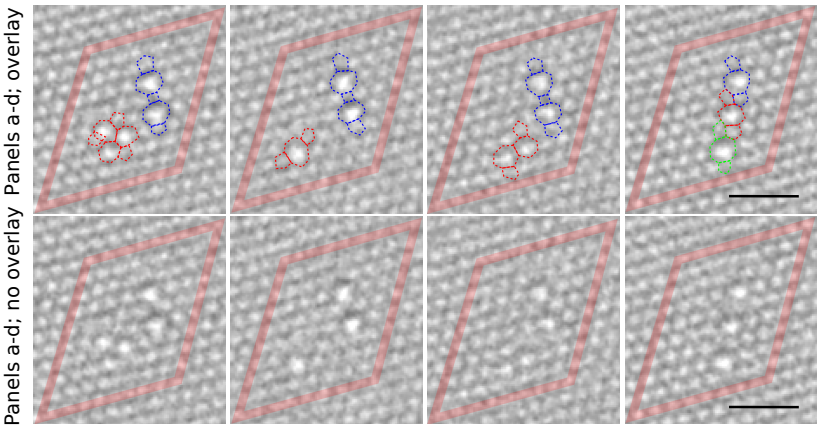

Figure 8. Panels a–d from Figure 3 of the main article with and without overlays. Scale bar is 1 nm.

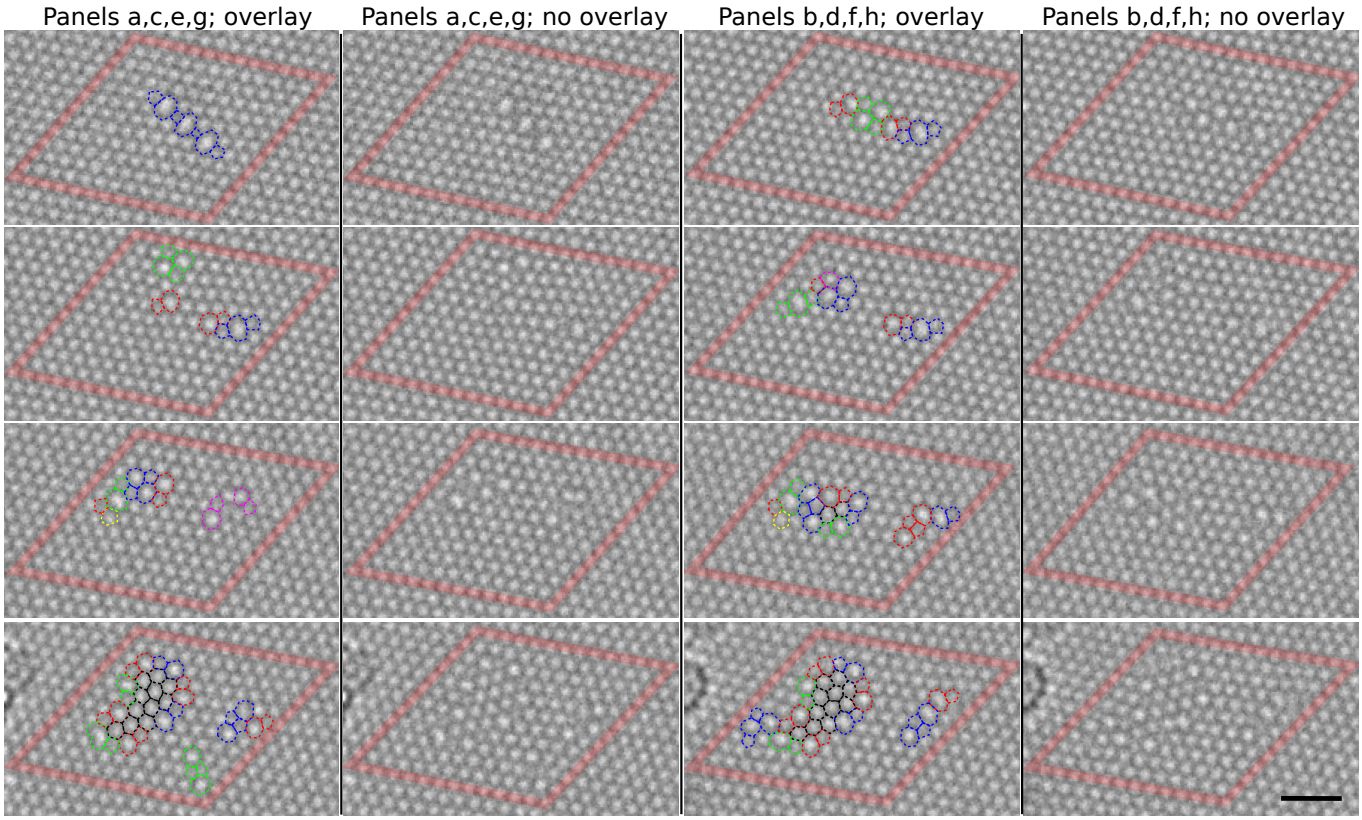

Figure 9. Panels a–h from Figure 4 of the main article with and without overlays. Scale bar is 1 nm.

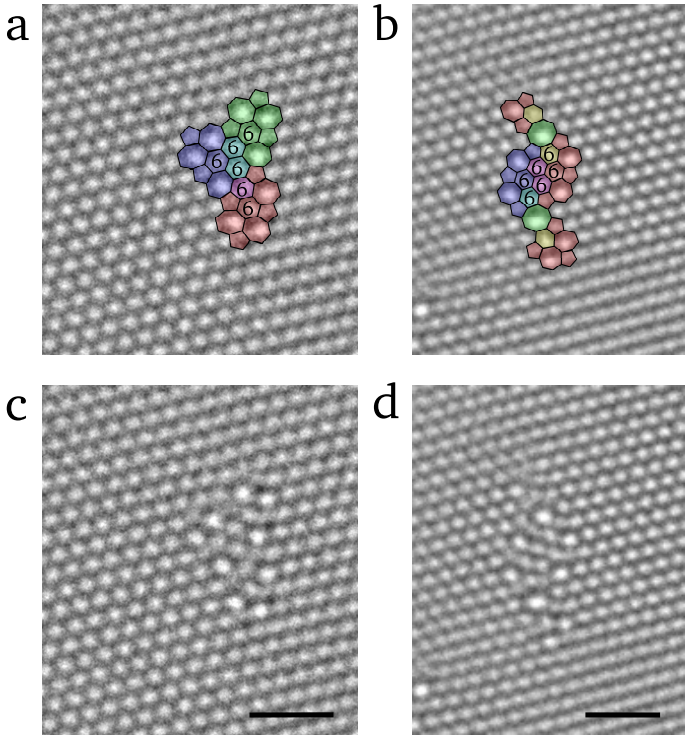

Figure 10. Two examples of defect structures created by short 300 keV exposure and imaged at 80 keV. In the upper row (panels a,b) DFT-optimized configurations are superimposed over the experimental images. Lower row (panels c,d) displays the structures without DFT-overlays. The first structure (a,c) can be constructed by combining three V_2(5555-6-7777) reconstructed di-vacancies (6 missing atoms), whereas the second one (b,d) can be formed from two V_2(5555-6-7777)'s, two V_2(5-8-5)'s, one V_2(555-777) and one (55-77) defect (total of 10 missing atoms), as indicated by the colors. Scale bars are 1 nm.